Journal of Catalysis 258 (2008) 35–43

Contents lists available at ScienceDirect

Journal of Catalysis

www.elsevier.com/locate/jcat

How important is the (001) plane of M1 for selective oxidation of propane to acrylic acid?

A. Celaya Sanfiz [a], T.W. Hansen [a], A. Sakthivel [a], A. Trunschke [a,*], R. Schlögl [a], A. Knoester [b], H.H. Brongersma [b], M.H. Looi [c], S.B.A. Hamid [c]

[a] Fritz Haber Institute of the Max Planck Society, Department of Inorganic Chemistry, Faradayweg 4-6, D-14195 Berlin, Germany
[b] Calipso B.V., P.O. Box 513, 5600 MB Eindhoven, The Netherlands
[c] COMBICAT, University Malaya, 50603 Kuala Lumpur, Malaysia

ARTICLE INFO

Article history:
Received 7 March 2008
Revised 22 May 2008
Accepted 23 May 2008
Available online 3 July 2008

Keywords:
MoVTeNb oxide catalyst
M1
Propane oxidation
Propane ammoxidation
Low-energy ion scattering
LEIS

ABSTRACT

The role of the (001) crystallographic plane of the M1 phase of MoVTeNb mixed-oxide catalysts in selective oxidation of propane to acrylic acid was addressed by investigating a phase-pure M1 material preferentially exposing this surface. A model catalyst was prepared by complete silylation of M1, followed by breakage of the SiO_2-covered needles. Using this approach, the reactivity of the M1 (001) surface was investigated by combining a microreactor study of propane oxidation with high-sensitivity low-energy ion scattering (HS-LEIS). Scanning electron microscopy (SEM) and transmission electron microscopy (TEM) were used to study the shape and microstructure of the model system and verify the surface exposure of the model catalyst. The specific rate of formation of acrylic acid on the model catalyst was found to be similar to that on the phase-pure M1 reference material, indicating that the (001) plane of the M1 crystal structure did not have better catalytic properties compared with the lateral surface of M1 needles in propane oxidation.

1. Introduction

Selective oxidation of light alkanes requires multifunctional catalysts capable of simultaneous activation of C–H bonds, insertion of oxygen atoms, and prevention of CO_x formation by further oxidation of intermediates or desired reaction products, which usually are much more reactive than the inactive reactant. The necessary functional diversity is implemented in chemically and structurally complex $MoVTeNbO_x$ catalysts, which show high activity and selectivity in partial (amm)oxidation of propane to acrylic acid and acrylonitrile, respectively [1,2]. Usually, these catalysts consist of phase mixtures composed of the so-called “M1” and “M2” phases [3], as well as minor amounts of phases such as Mo_5O_{14}-type structures or binary MoV and MoTe oxides. Propane activation and high selectivities toward acrylic acid and acrylonitrile generally are attributed to the presence of the orthorhombic M1 phase [4–6]. The M1 structure (ICSD 55097) consists of corner-sharing MO_6 octahedrons (M = Mo, V), which are assembled in the (001) plane forming characteristic hexagonal and heptagonal rings hosting Te–O units. Niobium is preferentially located in a pentagonal bipyramidal environment [7–9]; however, due to a certain chemical flexibility of the phase, octahedral positions also may be occupied by Nb in M1 with higher Nb content [10]. A bronze-like channel structure is established by stacking layers of the polyhedrons in the [001] direction, resulting in a needle-like crystal morphology in which the {001} planes are arranged perpendicular to the long axis of the needle. It has been suggested that terminating (001) planes of the M1 phase contain the active and selective surface sites for partial oxidation reactions [11–14]. This claim has stimulated research on the structure and properties of the M1 surface by low-energy ion scattering (LEIS) [15,16]. One unique feature of LEIS analysis is that it gives the atomic composition of the outermost atoms of a surface. These outer atoms are precisely the atoms that largely control the catalytic properties of the solid. It has been shown previously [17] that in cases where conventional surface analytic techniques, such as XPS, do not show correlation with the catalytic activity, the extreme surface sensitivity of LEIS gives a direct relationship between composition and catalysis. A recent review described the underlying principles behind and quantification of LEIS [18]. The general absence of matrix effects allows the use of simple reference samples for quantifying the surface composition.

The present study addresses the origin of the positive effect of grinding on the catalytic activity of MoVTeNb mixed oxides in the selective oxidation of propane to acrylic acid. Due to the needle-like shape of the particles, the surface area of (001) planes comprises only a minor fraction of the total surface area. Thus, increased activity after grinding of M1 needles has been attributed to the generation of additional (001) surface area [11,12]. Even though

* Corresponding author.
E-mail address: trunschke@fhi-berlin.mpg.de (A. Trunschke).

0021-9517/$ – see front matter
doi:10.1016/j.jcat.2008.05.028

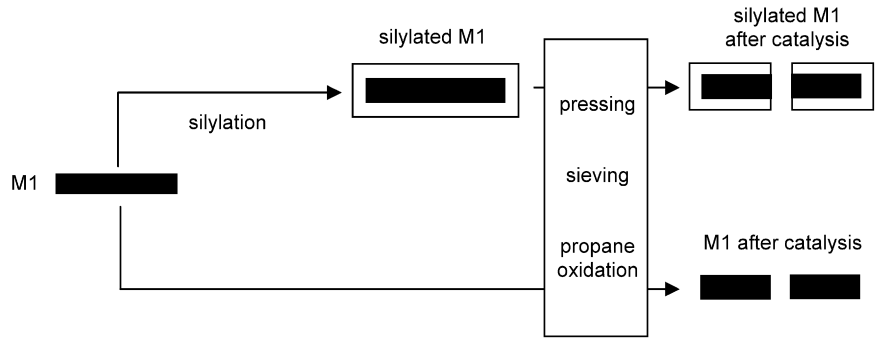

Scheme 1. Silylation and mechanical treatment of phase-pure M1.

an increased specific surface area is observed [12], the downside of the grinding process is the well-known effect of mechanical treatment on the nature and concentration of defects on the overall surface of transition metal oxides [19].

Consequently, here we have pursued a different strategy, as illustrated in Scheme 1. A batch of crystalline, phase-pure M1 prepared by hydrothermal synthesis was divided into two parts. One part was fully coated with silica. The complete coverage of the mixed-metal oxide surface by SiO_2 was verified by HS-LEIS. Both the coated material and the noncoated reference M1 were pressed into pellets, crushed, and sieved to prepare sieve fractions, which were then loaded into a microreactor and studied in the partial oxidation of propane to acrylic acid. Preparation of the sieve fraction represents a gentle mechanical treatment that generates new M1 surfaces, as was quantified by LEIS for the silica-coated catalyst [18] and by nitrogen adsorption for the reference material. Special attention was given to a comprehensive microstructural characterization of the model catalysts before and after propane oxidation. Scanning electron microscopy (SEM) and transmission electron microscopy (TEM) revealed that complete coverage of M1 followed by breakage of the SiO_2-covered needles generated a model catalyst that predominantly exposes (001) planes (Scheme 1). In addition, LEIS was applied to compare the chemical composition of the newly formed M1 surface of the coated catalyst with that of the total surface of the M1 reference. Based on the results of the microreactor and LEIS study, the relevance of particular surface terminations are discussed in view of the catalytic properties of phase-pure M1 catalysts in the partial oxidation of propane to acrylic acid.

2. Experimental

2.1. Preparation of M1

A phase-pure M1 catalyst with nominal atomic ratio Mo/V/Te/Nb = 1/0.3/0.23/0.13 was prepared starting from 18.71 g of MoO_3 (Fluka) suspended in 300 mL of bidistilled water. After the addition of 19.90 g oxalic acid at 363 K, a light-yellowish solution was obtained. The mixture was stirred for 25 min and then cooled to 313 K. Then 6.86 g of telluric acid (Sigma-Aldrich) dissolved in 30 mL of bidistilled water at 313 K was added to the molybdenum oxalate solution. A vanadium solution was synthesized by carefully mixing 7.05 g of oxalic acid and 3.55 g of V_2O_5 (Riedel–de-Haën) in 30 mL of bidistilled water at 338 K. The resulting blue solution was cooled to 313 K and added to the binary MoTe solution. Finally, a solution of 7.35 g ammonium niobium oxalate (Sigma–Aldrich) in 30 mL of bidistilled water was added to this mixture at 313 K. The clear quaternary solution was stirred for 10 min and then spray-dried in a Büchi B-191 spray-dryer at an inlet temperature of 423 K. The delivery rate of the pump and the aspirator were tuned to an outlet temperature of 383 K.

The spray-dried material was calcined in flowing air at 548 K (heating rate, 5 K/min) for 1 h. The calcined mixed oxide was then heated for 2 h at 773 K (heating rate, 5 K/min) and 20 MPa in the presence of steam. The resulting solid was finally crystallized to M1 in flowing argon at 873 K (heating rate, 15 K/min) for another 2 h (catalyst ID 3030). The atomic ratio of the metals in the final catalyst, Mo/V/Te/Nb = 1/0.34/0.08/0.14, as determined by EDX was close to the nominal ratio, with the exception of the reduced tellurium content due to evaporation of elemental Te during thermal activation of the catalyst.

2.2. Silylation of M1

Silylation of M1 was performed by adding 5.8 g of $HSi(OEt)_3$ (Sigma–Aldrich) to a suspension of 0.5 g of phase-pure M1 (catalyst 3030) in 100 mL of toluene. The mixture was kept for 16 h at 384 K under reflux. Cross-linking of anchored silanol groups was achieved by treating the resulting solid in a mixture of 90 mL of ethanol, 10 mL of bidistilled water, and 1 mL of concentrated sulphuric acid for 4 h under reflux. The two-step procedure was repeated three times to ensure complete silylation of the entire M1 surface (catalyst ID 3159).

2.3. Activity measurements

For testing of the catalysts in selective oxidation of propane to acrylic acid, 0.5 g of each material was pelletized (8 ton on a round, 3-cm-diameter surface) and sieved to 200–400 μm. This shape-forming procedure, referred to as mechanical treatment, causes partial disruption of the needles, changing the size distribution of the primary particles in the original M1 and making catalytic testing of completely silylated M1 impossible. But pure silica (Aerosil 300) was shown to be inactive in propane oxidation under the reaction conditions applied. The sieve fractions of the mechanically treated M1 and silylated M1 were loaded into quartz reactors with a diameter of 4 mm. The feed was composed of propane/oxygen/nitrogen/steam in a molar ratio of 0.85/1.9/15.2/12. The reaction was performed at atmospheric pressure, a GHSV of 4800 h^{-1}, and a reaction temperature of 673 K. The products were analyzed by gas chromatography. A molecular sieve column and a Porapak column coupled with a thermal conductivity detector were used to analyze O_2, N_2, CO, CO_2, and hydrocarbons (C_1–C_3). The oxygenated products were analyzed with a HP-FFAP column coupled with a flame ionization detector. The detection limit of the individual products depended on the detector used but was generally >0.2 vol%. A mass balance of 100 ± 10% was calculated.

2.4. X-ray diffraction

The phase purity of the materials was verified by X-ray diffraction (XRD) using a STOE STADI-P transmission diffractometer

Table 1
Results of particle shape analysis based on SEM images and BET surface areas measured by nitrogen adsorption

Catalyst	Number of particles	l_{mean} (nm)	d_{mean} (nm)	d/l	Calculated[a] total surface area of one needle (nm^2)	Calculated[a] surface area of the (001) plane of one needle (nm^2)	Calculated[a] specific surface area (m^2/g)	BET surface area (m^2/g)
M1[b]	379	336 ± 189	184 ± 99	0.56	2.47×10^5	0.53×10^5	6.3	6.7
M1[c]	241	277 ± 119	164 ± 85	0.59	1.85×10^5	0.42×10^5	7.2	7.6
Silyl. M1[c]	298	275 ± 114	167 ± 71	0.61	1.88×10^5	0.44×10^5	7.1	n.d.

[a] Calculation under consideration of mean diameter, mean length and under assumption of cylindrical geometry with circular basal plane.
[b] M1 as synthesized.
[c] Catalyst after propane oxidation.

equipped with a focusing primary Ge (111) monochromator and a position sensitive detector, using Cu$K\alpha_1$ radiation. For data analysis, the Topas program, v.2.1 (Bruker AXS) was used to fit the diffraction patterns of the activated materials.

2.5. Electron microscopy

The microstructure of the catalysts was investigated by TEM using a Philips CM 200 FEG transmission electron microscope operated at 200 kV, equipped with a Gatan CCD camera for image acquisition and an EDAX Genesis EDX system. Morphology studies and shape analysis were performed by SEM, using a Hitachi S-5200 with a PGT Spirit EDX system and a Hitachi S-4800 with an EDAX Genesis EDX detector. EDX studies in the SEMs were carried out with an accelerating voltage of 10 kV, with images acquired at 2 kV to optimize surface resolution. For TEM, the specimens were prepared by dry dispersing the catalyst powder on a standard copper grid coated with holey carbon film. For SEM investigations, the samples were deposited on carbon tape. The shape of the M1 needles was analyzed by measuring the length and diameter of more than 200 needles on SEM images. Based on the average length and diameter of the needles, the total surface area and the surface area of the (001) plane were calculated for an average needle for each catalyst (Table 1). These calculations were done under the assumptions that the material was 100% crystalline and each crystal was cylindrically shaped. Furthermore, the cylinder was assumed to have a circular basal plane. A SEM-derived specific surface area was calculated using the surface area of the average needle and the crystallographic density of M1 (4.4 g/cm^3 [8]).

2.6. Nitrogen adsorption

The specific surface areas of the catalysts were measured using an AUTOSORB-1-C physisorption/chemisorption analyzer (Quantachrome). Eleven points in the linear range of the nitrogen adsorption isotherm measured at 77 K were used to calculate the BET surface area. Before adsorption, the samples were degassed at 353 K for 2 h.

2.7. High-sensitivity LEIS

The Calipso LEIS uses a double toroidal analyzer, which combines a large acceptance angle with parallel energy analysis of the backscattered ions. This gives orders of magnitude higher sensitivity (HS-LEIS) than that of conventional LEIS equipment [20]. The required ion dose for analysis is so low that HS-LEIS analysis is essentially nondestructive ("static").

The extreme surface sensitivity of LEIS requires that organic contaminations due to transport and storage as well as carbonaceous deposits from the catalytic reactions be removed from the catalysts before analysis. This was done with an oxygen atom source (Oxford Applied Research, type MPD 21) that produces O-atoms of thermal energy. In contrast to molecular oxygen and ozone, the chemical energy of these O-atoms enables the complete removal of organic contaminations at room temperature without sputtering the surface. All samples were cleaned in this manner (200 W, 5 min) before analysis. Prolonged treatment had no influence on the LEIS spectra, confirming the cleanliness of the samples.

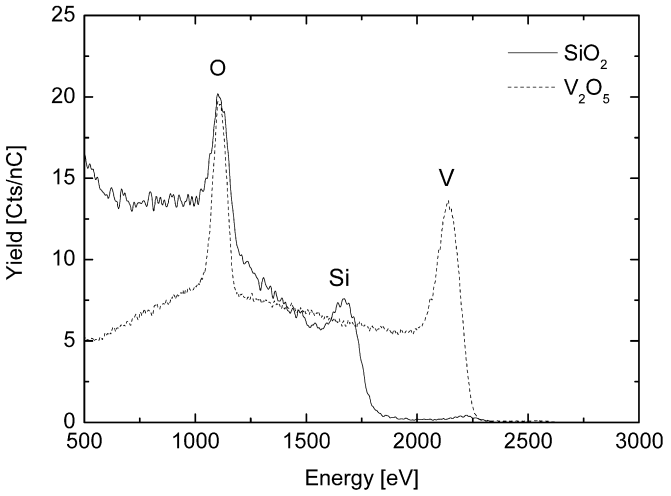

Fig. 1. 3 keV He^+ scattering. References SiO_2 and V_2O_5.

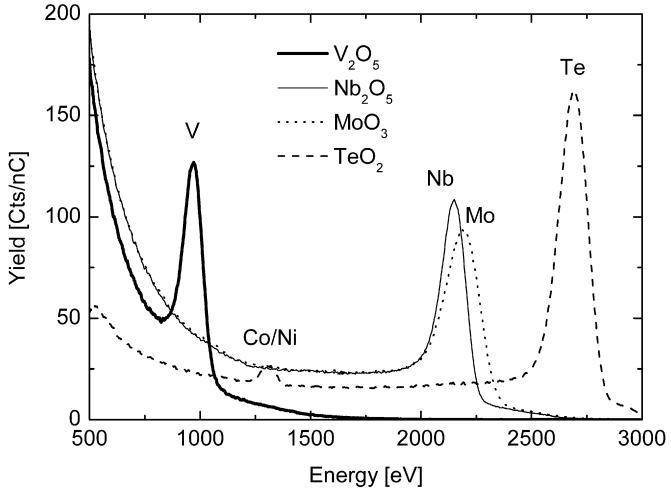

Fig. 2. 5 keV Ne^+ scattering. references V_2O_5, Nb_2O_5, MoO_3 and TeO_2.

2.8. Calibration of the LEIS signals

It has been shown previously that roughness has a very small effect on the LEIS signals [21]. Thus, the precise dispersion is not of great importance for a good reference for calibrating the LEIS signals of the catalysts. Thus, high-purity powder samples of SiO_2, V_2O_5, Nb_2O_5, MoO_3, and TeO_2 were used as references to quantify the surface concentrations of Si, V, Nb, Mo, and Te. Because the surfaces were cleaned with O atoms, the cations in the outer sur-

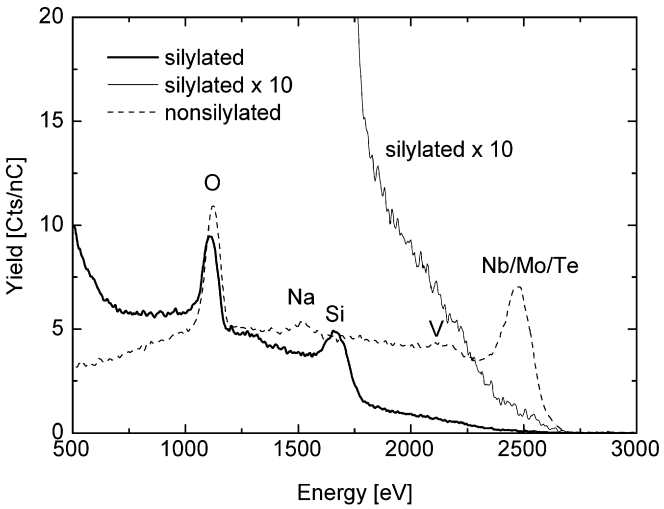

Fig. 3. 3 keV He^+ scattering. Nonsilylated, silylated and silylated × 10.

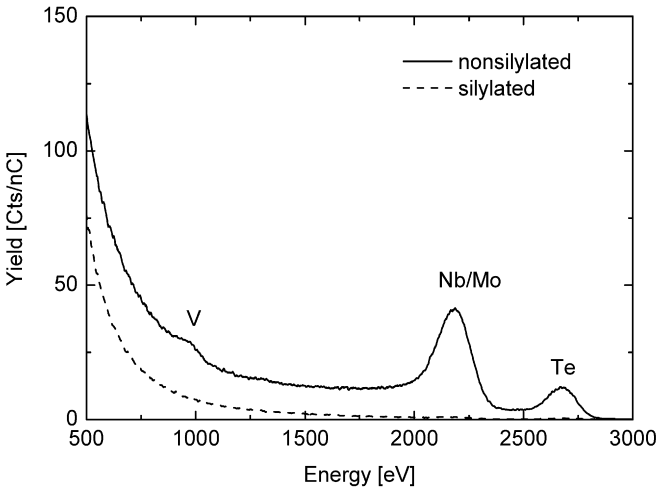

Fig. 4. 5 keV Ne^+ scattering. Nonsilylated and silylated.

face were in their highest oxidation state (e.g., TeO_3 for Te). The LEIS spectra are given in Figs. 1 and 2. The lighter elements (Si, V) were quantified with 3 keV $^4He^+$ ions; the heavier elements (V, Nb, Mo and Te), with 5 keV $^{20}Ne^+$ ions. As can be seen in Figs. 1 and 2, the SiO_2 surface was contaminated with a trace of iron oxide, whereas the TeO_2 contained some cobalt or nickel oxide (mass 59). Even with the heavier Ne ions, there was an overlap of the Nb and Mo peaks. The elements are neighbors in the periodic table, and their isotopes (Nb: 93; Mo: 92–100) overlap. For the catalysts, the relative concentrations of Nb and Mo were determined by curve fitting. The large width of the Te peak originates from isotopic broadening (atomic mass 122–130). Because these masses are very different from those of the other elements, Te can be readily quantified. V can be analyzed using both He and Ne ions, and the two analyses give very similar results. The values given for V are the average of the two measurements.

LEIS calibration gives the fractions of the surface that are composed of the various oxides. To obtain atomic concentrations, these fractions must be corrected for the surface densities of the cations in the references. These surface densities have been estimated as $(\rho \cdot N_{Av}/M)^{2/3}$, where ρ is the bulk density, N_{Av} is Avogadro's number, and M is the molar mass. It has been shown previously [22] that this estimate agrees closely with the estimate from the surface unit-cell taking the close-packed surface plane, which is dominant on powders. For V_2O_5, Nb_2O_5, MoO_3, and TeO_3 these densities are 9.96, 9.36, 7.28, and 7.68 ($\times 10^{14}$) metal atoms/cm^2, respectively.

3. Results

3.1. Silylation of M1

The surface of a $MoVTeNbO_x$ mixed oxide composed mainly of the M1 phase was covered with a layer of silica by silylation using $HSi(OEt)_3$. The silylation was optimized using LEIS. Figs. 3 and 4 show the LEIS spectra of the catalyst before and after silylation according to the process described in Section 2. The 3 keV He^+ spectrum before silylation shows peaks for O and V and a combined peak for Nb, Mo, and Te, along with some Na contamination. The 5 keV Ne^+ spectrum gives a better mass resolution for the heavier elements. It shows the peaks for V and Te along with a broad peak due to Nb and Mo. After silylation, only the peaks for O and Si (He spectrum) are present. No peaks are observed in the Ne spectrum. This confirms complete silylation of the catalyst.

In addition to the peaks in the He spectrum, a background extending to higher energies can be seen, due to ions that were backscattered by Nb and Mo/Te in deeper layers. The most likely process for this is that the ions were neutralized at the initial interaction with the surface; lost some energy along the ingoing (straggling) trajectory; backscattered in a hard binary collision with a Nb, Mo, or Te atom; and lost some more energy while straggling back to the surface. Because only backscattered ions are detected in LEIS, the backscattered He atoms must be reionized in an interaction with a surface atom just before leaving the surface. For 3 keV He^+ ions scattered by this type of oxide, the straggling energy loss contributes about 160 eV for backscattering from a depth of 1 nm. The shape of the 10× magnified background thus gives information on the thickness distribution of the silica coating. It shows that a small fraction of the coating is only just covered (1–2 atoms thick), while the maximum thickness is about 2 nm. Consistently, TEM (see below) shows that the silica layer is not homogeneous, and that its thickness varies.

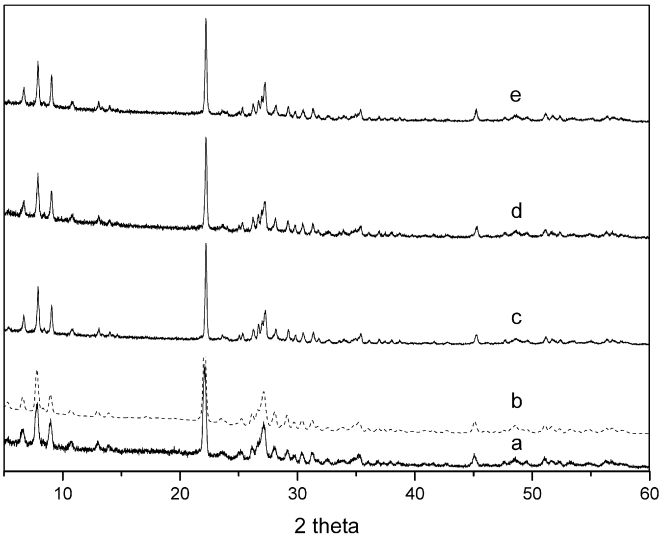

Fig. 5. XRD patterns of as synthesized M1 (a), and calculated patterns assuming phase-pure M1 [8] (b); XRD patterns of M1 after propane oxidation (c), and of silylated M1 before (d) and after (e) propane oxidation.

3.2. Phase composition of the MoVTeNb oxide

In regard to the bulk structure, a material of high phase purity was exposed to the silylating agent (Fig. 5a), as is evident from comparing the measured XRD patterns with the patterns calcu-

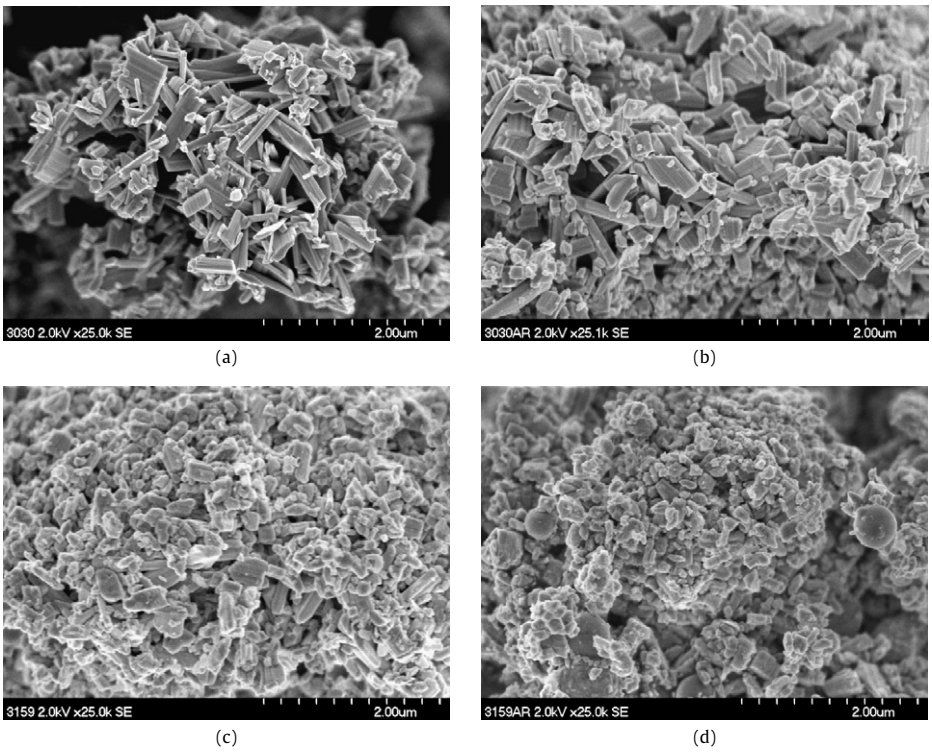

Fig. 6. SEM images of phase-pure M1 before (a) and after propane oxidation (b); SEM images of silylated M1 before (c) and after propane oxidation (d).

lated under the assumption that the solid is composed exclusively of M1 [8] (dotted line in Fig. 5b). Within the method's range of accuracy, the material is phase-pure. The phase composition of the mixed oxide remained unchanged after catalytic reaction (Fig. 5c) and also after the silylation procedure (Figs. 5d and 5e). The materials are highly crystalline, as also confirmed by TEM.

3.3. Microstructure of the model catalysts

The typical needle-shape morphology of the original phase-pure M1 material is observed in the SEM image shown in Fig. 6a. Only very few particles are found that clearly differ in morphology, indicating the presence of traces of other phases not detectable by XRD or minor amounts of amorphous fractions. The needle-shape morphology is maintained after catalytic testing (Fig. 6b) and after silylation (Fig. 6c). In the latter material, some spherical particles are observed that have been assigned to pure SiO_2 by EDX analysis. The needle-like shape of the silylated M1 particles (Fig. 6c) also is not significantly affected by propane oxidation (Fig. 6d).

Shape analysis of the original M1 catalyst reveals a broad distribution of the needle length with a maximum between 100 and 400 nm (Fig. 7a). The abundance of shorter needles, especially those with length shorter than 400 nm, clearly increases after propane oxidation (Fig. 7b), which is attributed to breakage of the needles due to mechanical manipulation during preparation of the sieve fraction before the catalytic test. A similar length distribution is seen with the silylated catalyst after the catalytic reaction (Fig. 7c), indicating a comparable impact of mechanical treatment for silylated and nonsilylated M1.

Table 1 summarizes mean needle length, mean needle diameter and the mean diameter/length ratio of the needles obtained by shape analysis of about 300 needles for the original M1 material, the M1 catalyst after propane oxidation, and the silylated M1 after catalytic testing. Because the M1 needles are naturally crystals with a preferred growth direction perpendicular to the {001} planes, a preferential breaking perpendicular to the length axis would be expected during mechanical treatment. This preferential breaking is reflected in a slight increase of the mean diameter/length ratio from 0.56 for the original M1 catalyst before propane oxidation to 0.59 and 0.61 for the nonsilylated and the silylated M1, respectively, after propane oxidation. Assuming that all needles have cylindrical geometry with circular basal planes and mean geometric parameters (diameter, length) as given in Table 1, the total surface area and the surface area of the (001) planes of an average needle have been calculated for the three model catalysts (Table 1). Taking into account a unit cell density of M1 of 4.4 g/cm^3 [8], specific surface areas can be calculated that agree well with the BET surface areas measured (Table 1), confirming the high crystallinity of the materials. If each needle were disrupted once, an increase in surface area of about 20% would be expected from the cylindrical geometry. The actual increase in BET

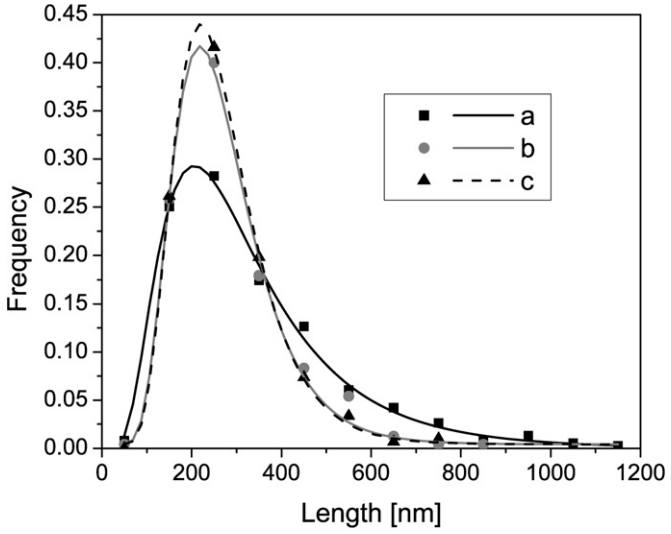

Fig. 7. Distribution of the needle length in as synthesized phase-pure M1 (a), in M1 after propane oxidation (b), and in silylated M1 after propane oxidation (c).

surface area of the nonsilylated M1 before and after propane oxidation of 13% agrees well with the increase in specific surface area of 14% calculated based on the shape analysis, confirming the reliability of the method. The BET surface area of the silylated M1 was not measured because it was expected that the presence of silica particles would falsify the result. However, considering the similar size distribution of nonsilylated and silylated needles after the catalytic testing (Fig. 7), an increase in surface area of 13% could be expected for the silylated catalyst as well.

In summary, the combined shape and BET surface area analysis clearly indicate a preferential disruption of the M1 needles perpendicular to the [001] direction by mechanical treatment before catalytic testing. Comparing nonsilylated and silylated M1 needles, the similar impact of the mechanical treatment on particle morphology provides further evidence for the applicability of the present approach.

Provided that no silica is removed from the sides of the needles, the new surface area formed by mechanical treatment of completely silylated M1 is composed mainly of (001) planes (Scheme 1). Needles that exclusively expose the (001) plane have been detected by high-resolution transmission electron microscopy in the silylated M1 catalyst after the catalytic test reaction (Fig. 8a). The image in Fig. 8a shows one needle with the sides covered by silica and with the cross-sectional plane free of SiO_2, confirming that the needles can break perpendicular to the longitudinal axis. Furthermore, needles completely covered by a layer of silica are also seen (Fig. 8b), indicating that not every needle is broken. This is in agreement with the results of shape analysis and nitrogen adsorption. The possibility of partial removal of silica from the sides of the needles cannot be excluded, as evidenced by the TEM image shown in Fig. 8c.

3.4. Catalytic properties of the model catalysts in propane oxidation

Pure silica shows no catalytic activity in propane oxidation under the reaction conditions applied. Thus, completely silylated M1 is expected to be inactive. But experimentally verifying this statement for a completely silylated model catalyst is impossible. Mechanical manipulation of the catalyst by pressing and sieving is required to prepare a sieve fraction before catalytic testing. This causes partial damage of aggregates and even of the primary particles, resulting in exposure of a new $MoVTeNbO_x$ surface in both the silylated and nonsilylated reference catalysts (Scheme 1).

Table 2 compares the catalytic performance of the two mechanically treated catalysts. Propane oxidation was performed in parallel reactors with the same temperature, space velocity, and feed composition. Under steady-state conditions, the conversion of propane is fivefold greater over the reference M1 than over the silylated model catalyst. Whereas only acrylic acid is formed over silylated M1, the selectivity is lower for the reference material, producing 12% CO_2 and 15% CO as byproducts. These differences in selectivity most likely are related to the different propane conversion levels. The carbon oxides may be formed in consecutive reactions, thus lowering the selectivity to acrylic acid over the reference M1. Table 2 gives average rates. Due to the high conversion of the nonsilylated reference catalyst, the average consumption rate of propane is underestimated for this catalyst. Nevertheless,

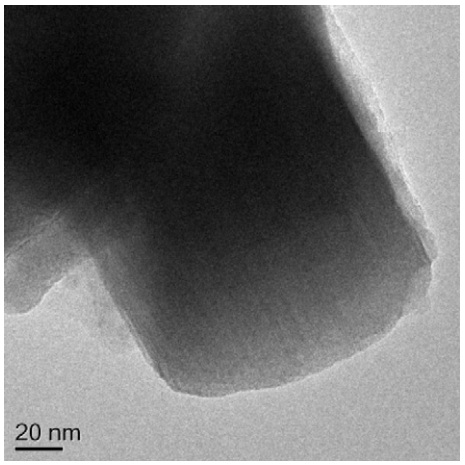

(a)

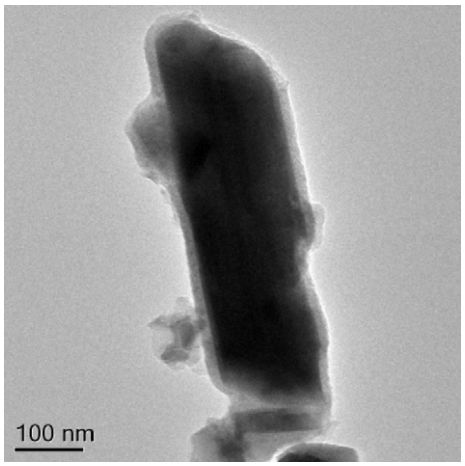

(b)

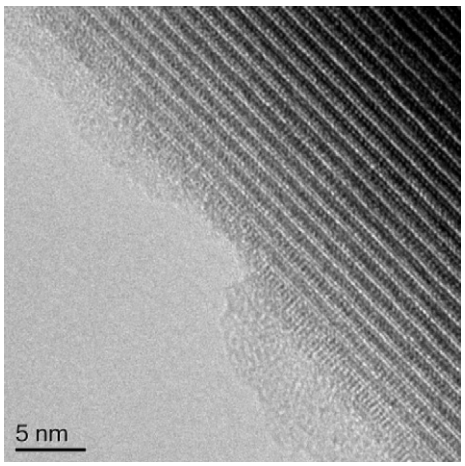

(c)

Fig. 8. HRTEM images of a silylated M1 needle disrupted along the (001) plane (a), of a completely silylated M1 needle (b), and of a silylated M1 needle with silica scratched from the sides (c).

Table 2
Catalytic properties of M1 and silylated M1 in propane oxidation to acrylic acid (AA) after 32 h time on stream at 673 K

Catalyst	$X_{C_3H_8}$ (%)	S_{AA} (%)	Y_{AA} (%)	C_3H_8 consumption rate		Formation rate AA	
				$mmol_{C_3H_8}/(h\,g_{cat})$	$mmol_{C_3H_8}/(h\,m^2_{exp.surf.})$	$mmol_{AA}/(h\,g_{cat})$	$mmol_{AA}/(h\,m^2_{exp.surf.})$
M1	49	73	36	>2.94	>0.39	>2.15	>0.28
Silylated M1	9	100	9	0.54	0.24	0.54	0.24

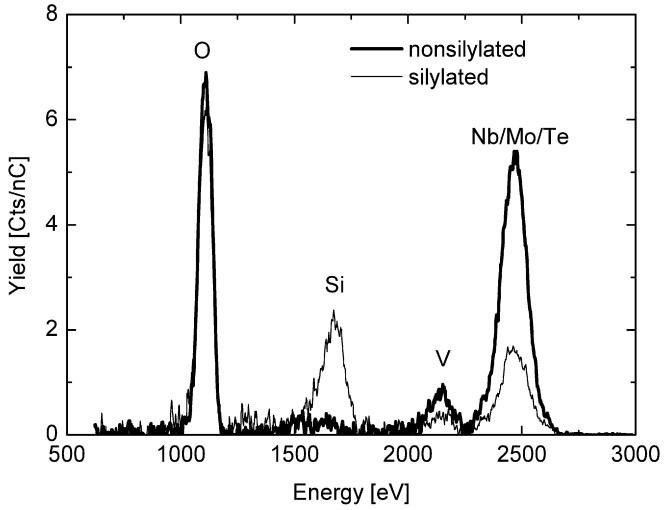

Fig. 9. Background-subtracted 3 keV $^4He^+$ spectra from catalytically tested samples.

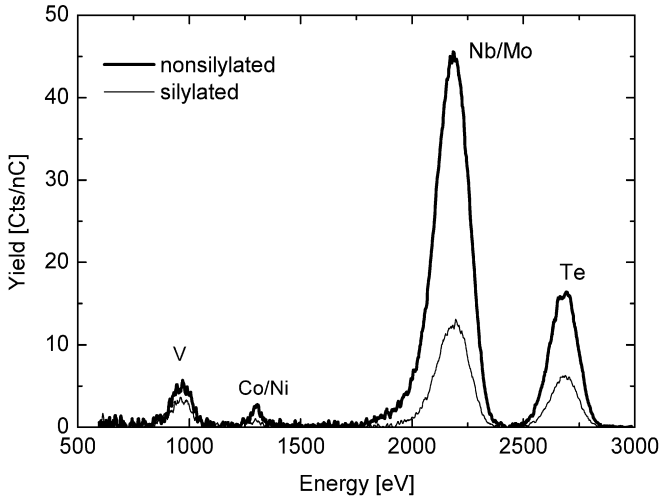

Fig. 10. 5 keV $^{20}Ne^+$ spectra from catalytically tested samples.

it is fivefold greater than that of the silylated catalyst. The larger $MoVTeNbO_x$ surface area that is exposed to the reactants in case of the nonsilylated reference catalyst is a possible explanation for this finding. The surface area of the reference M1 was measured by nitrogen adsorption (Table 1). LEIS was used to determine the accessible $MoVTeNbO_x$ surface area of the silylated catalyst, as described in the following section.

3.5. LEIS after catalysis

To properly compare the catalysts, the silylated and nonsilylated samples were both investigated with LEIS after the same mechanical treatment (pelletizing, crushing, sieving) and catalytic testing (see Scheme 1). Figs. 9 and 10 show the He and Ne spectra after background subtraction. Due to partial disruption of the needles, significant signals can be seen for V, Nb, Mo, and Te in the silylated sample. Again, some Co/Ni contamination is present. The surface fractions of the elements in Figs. 9 and 10 can be quantified using the reference spectra in Figs. 1 and 2. It is seen that the sum of the surface fractions of V_2O_5, Nb_2O_5, MoO_3, and TeO_3 in the treated silylated sample amounts to 30% of that in treated nonsilylated sample. The other part of M1 (70%) remains covered by SiO_2. The 30% thus represents the new surface generated by the mechanical treatment.

Table 3
Metal composition of the bulk (EDX) and topmost layer (LEIS) in at%. The numbers in parentheses represent molar ratios of the metals normalized to molybdenum

Catalyst	Method	Mo	V	Te	Nb
M1[a]	EDX	64 (1)	22 (0.34)	5 (0.08)	9 (0.14)
	LEIS	n.d.	n.d.	n.d.	n.d.
M1[b]	EDX	64 (1)	20 (0.31)	6 (0.09)	10 (0.16)
	LEIS	65 (1)	12 (0.18)	12 (0.18)	11 (0.17)
Silylated M1[a]	EDX	63 (1)	22 (0.35)	6 (0.09)	9 (0.14)
	LEIS	0	0	0	0
Silylated M1[b]	EDX	62 (1)	21 (0.34)	6 (0.09)	11 (0.18)
	LEIS	55 (1)	20 (0.37)	15 (0.27)	10 (0.17)

[a] As synthesized.
[b] Catalyst after propane oxidation.

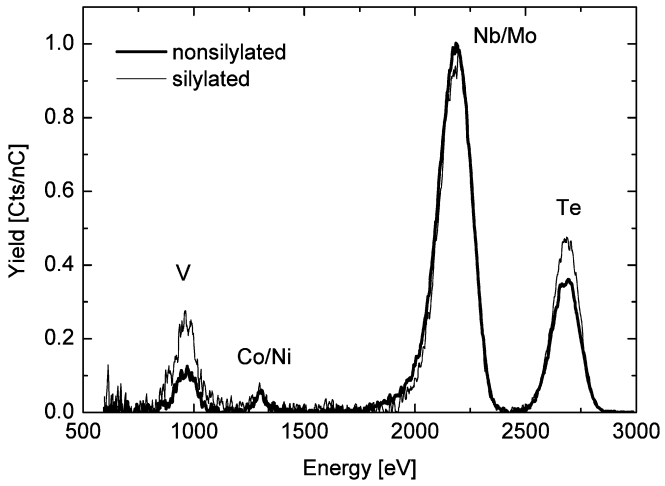

Fig. 11. Normalised 5 keV $^{20}Ne^+$ spectra (Mo = 1.00) from catalytically tested samples (after subtraction of background).

To obtain the atomic surface concentrations, the surface fractions of the oxides must be corrected for the differing metal atoms/cm^2 in these oxides. Table 3 gives the atomic compositions (in parentheses normalized to Mo) for the treated nonsilylated sample and the new surface of the silylated sample, along with the results of the bulk analyses by EDX for comparison. In agreement with earlier studies [15], the chemical composition of the outermost surface layer differs significantly from that of the bulk. The LEIS measurement of the M1 reference provides important information, including the basal plane and the lateral surface, showing an enrichment of tellurium at the expense of vanadium. The situation on the freshly formed surface of the silylated model catalyst, which is dominated by the (001) plane, is different, with an increase in tellurium at the expense of molybdenum. No depth profile and no differences between the catalysts with respect to the Nb concentration are noted. Fig. 11 also illustrates the clear differences in the surface compositions, with the Ne spectra normalized on the maximum of the Nb/Mo peak.

4. Discussion

It has been well documented that the M1 phase occurring in MoVTeNb mixed-oxide catalysts plays a key role in the selective oxidation and ammoxidation of propane [6,14,23]. The crystal structure hosts four different metals, three of them with variable oxidation states, meeting the requirements for catalyzing redox reactions by exposing or bearing structural arrangements at the surface that easily meet the demands of propane activation and the transfer of 8 electrons in its selective oxidation to acrylic acid or in its ammoxidation to acrylonitrile, respectively. Surface and sub-

surface reduction and reoxidation of M1 crystals without structural collapse seem to be possible [24]. The occupancy of the 13 metal sites in the unit cell of the crystal structure is variable [9,10,14]. Accordingly, the catalytic properties may be controlled by synthesis or posttreatment procedures. Crystallinity seems to be required to obtain catalytic activity for selective (amm)oxidation of propane [6,25,26]. The possible role of defects remains an open question [24,27]. Typically, nanocrystalline M1, composed of fine needles a few hundred nanometers long, exhibits excellent catalytic behavior.

The phase-pure M1 synthesized in the present study exhibits the corresponding morphology and has very small amounts of impurity phases or amorphous fractions, as evidenced by XRD (Fig. 5) and electron microscopy (Fig. 6a). Compared with published M1 stoichiometries (e.g., $Mo_1V_{0.15}Te_{0.12}Nb_{0.13}O_x$ [8] or $Mo_1V_{0.23}Te_{0.11}Nb_{0.14}O_x$ [9]), the present material is characterized by increased V content and reduced Te content (Table 3), which may be the reason for its exceptional catalytic behavior (Table 2). The average formation rate of acrylic acid measured in the stationary state after 32 h on stream is 2.15 mmol/($h\,g_{cat}$), which exceeds the rates reported for M1 in the literature [28]. In preparing a model catalyst with preferentially exposed {001} planes we have chosen the present material due to its high phase purity and high catalytic activity. Based on grinding experiments, and under the assumption that the structural characteristics and the chemical composition of the surface do not differ from the bulk even under reaction conditions, it was previously concluded that the catalytically active sites in propane oxidation [11,12] or ammoxidation [14,26] are located on terminating (001) planes. This assumption is not consistent with room temperature LEIS measurements that give an indication of gradients in elemental composition between surface and bulk of M1 [29]. Surface texturing of catalyst particles also has been revealed by high-resolution TEM on the surface of high-performing $MoVTeNbO_x$ catalysts that have been leached with solvents [27]. In any case, a well-defined and rigid arrangement of structural units may be rather unlikely at the reaction temperature and in the presence of steam in the feed.

Exploring this question by in situ spectroscopic methods is quite challenging, however. Thus, in the present study we used propane oxidation itself as a probe reaction to ascertain the specific catalytic activity of the (001) plane compared with the integral activity of the entire M1 surface. For this purpose, the M1 crystals were covered completely by a thin layer of silica. HS-LEIS confirms coverage of the whole mixed oxide surface (Fig. 4). The thickness of the layer ranges from a few monolayers to 20 nm, as verified by LEIS and TEM. Neither the particle size distribution of the original M1 (Table 1) nor its chemical composition (Table 3) is affected by the silylation procedure. But the powders were pelletized, crushed, and sieved before being introduced into the catalytic test reactor. Such a gentle mechanical treatment leads to partial disruption of needles and formation of fresh $MoVTeNbO_x$ surface. For the silylated M1, the newly emerging MoVTeNb oxide surface was verified by HS-LEIS (Figs. 9 and 10). For the pure, nonsilylated M1, these morphological changes should be reflected in an increased specific surface area as measured by nitrogen adsorption. Under the assumption that the mechanical treatment leads exclusively to breakage of needles perpendicular to the [001] direction, the difference corresponds to the surface of newly formed (001) planes. In the present experiment, the difference in the specific surface area is 13.4% (Table 1). A very similar result (14.3%) is obtained if the mean particle size determined based on the shape analysis by SEM and the bulk density of M1 (4.4 g/cm^3 [8]) are used to calculate the increase in surface area of pure, nonsilylated M1 (Table 1), satisfactorily confirming the reliability of the shape analysis and demonstrating that the mechanical treatment applied is associated mainly with breakage of needles and not with any other damage. The relevance of shape analysis is important, because in the silylated catalyst, BET surface area measurements cannot be relied on for calculation due to an expected increase in surface area caused by the possibly not smooth SiO_2 layer and the occasional formation of pure silica particles.

Both the original M1 needles and the silylated needles have a low probability of breaking (Table 1, Fig. 7), and long needles break more frequently than short needles (Fig. 7). Fig. 7 confirms that nonsilylated and silylated needles break in a similar way, because the two materials have essentially the same particle size distribution after the catalytic test. For the silylated catalyst, the increase in surface area (i.e., the yield in newly formed basal plane surface area) corresponds to 12.7% when the mean particle size determined by shape analysis is used for the calculation (Table 1).

In summary, based on shape analysis and/or nitrogen adsorption before and after catalytic testing, the breakage of the M1 needles benefits in newly formed (001) surface area of approximately 15% for both the original and the silylated M1.

As an independent method, LEIS analysis was applied to determine the freshly formed $MoVTeNbO_x$ surface of the silylated catalyst. This fraction corresponds to 30% of the surface of the original M1. This value is twice as high as the increase calculated from the shape analysis, implying that more than silica-free (001) planes were generated. HRTEM (Fig. 8c) shows that some silica was scratched from the sides of the needles as well. Assuming that the approximate 15% increase in surface area calculated from shape analysis (Table 1) corresponds exclusively to the newly formed silica-free (001) planes, the ratio of the basal plane area versus other $MoVTeNbO_x$ surface area (i.e., lateral surface area) is about 1 in the silylated M1. In the original M1, the entire surface of the needles is exposed to the gas phase during propane oxidation and, thus the ratio of (001) surface area to lateral surface area corresponds to 0.25 (Table 1). Consequently, even though other surface planes also are to some extent exposed to the reactants in the silylated M1 during propane oxidation, we can conclude that the silylated, mechanically treated M1 catalyst represents a suitable model system for studying the catalytic properties of the (001) plane, because half of the exposed $MoVTeNbO_x$ surface is composed of (001) planes.

Table 2 compares the catalytic performance of M1 and silylated M1. As expected, the conversion of silylated M1 is much lower than that of M1, because less $MoVTeNbO_x$ surface is accessible in the former catalyst. Based on the information obtained from the HS-LEIS study indicating that actually 30% more $MoVTeNbO_x$ surface is available in the silylated catalyst, consumption rates of propane normalized to the area of exposed $MoVTeNbO_x$ surface were calculated considering a 7.6 m^2/g $MoVTeNbO_x$ surface for M1 (BET surface area given in Table 1) and a 2.3 m^2/g $MoVTeNbO_x$ surface for silylated M1 (0.30×7.6 m^2/g). The rates are quite similar for both catalysts, meaning that the intrinsic catalytic properties of the entire M1 surface are similar to the catalytic behavior of a surface composed of 50% (001) planes. This finding casts some doubt on the uniqueness of the basal plane of M1.

The result is especially surprising considering that the chemical composition of the newly formed M1 surface of the silylated catalyst (previously unexposed surface of M1) has a different chemical composition than the average surface composition of M1, as shown by the LEIS experiment. Table 3 compares the bulk composition measured by EDX and the surface composition measured by HS-LEIS. Whereas the EDX bulk compositions of the samples are almost the same, confirming that the silylation procedure does not affect the bulk composition, the HS-LEIS surface composition of the newly generated surface shows relatively large differences, specifically an increased concentration of tellurium at the expense of molybdenum. However, prior to the present LEIS measurements, a mild pretreatment with oxygen atoms at room temperature was

necessary to eliminate environmental contamination from the reaction, transport, and storage. This procedure, which converts all of the surface metal ions into their highest oxidation states, may be connected with structural changes. Although the local structure is affected, it is unclear whether the elemental composition changes significantly. However, the surface reconstruction holds for the entire surface of M1, thus justifying a comparison of the basal plane with the total surface in terms of elemental composition.

In any case, these uncertainties do not affect the findings that the intrinsic catalytic properties of the basal plane of M1 in the selective oxidation of propane to acrylic acid do not differ much from those of the lateral surface of the M1 needles. If we accept this result, then the question arises as to why increased catalytic activity and improved selectivity to acrylic acid were observed in previous studies after grinding of M1 [11,12]. The details of the grinding procedure were not given in those reports; however, most likely the mechanical treatment was less gentle than that in the present study and probably generated a more defect-rich material along with extra basal planes. Another possible explanation could be that contamination, such as residues from the preparation procedure, which are common on catalyst surfaces, were removed by extended grinding. Breaking the needles and scratching deposited impurities away from the sides of the needles would expose fresh, uncontaminated, and thus active MoVTeNb oxide surface.

5. Conclusion

The model studies presented here suggest that a distinguished lattice plane of the M1 crystal structure, the (001) plane, is not solely responsible for its outstanding catalytic activity and selectivity in the partial oxidation of propane to acrylic acid. The chemical and structural natures of the active ensembles on the catalyst surface remain unknown. The unique crystal structure of the M1 phase certainly plays an essential role in the selective (amm)oxidation of propane, because amorphous material or MoVTeNb oxide comprising different phases cannot compare with phase-pure crystalline M1. All experimental experience to date suggests that this may differ from the situation for related mixed oxides, such as nanostructured MoVW oxides, which have been reported to be active in propylene oxidation in a semicrystalline state [30]. Similar intrinsic reactivity irrespective of the terminating lattice plane implies that related active ensembles of metal–oxo clusters are exposed to the reactants on the entire surface of the M1 needles. The lateral surface of the needles accounts for the main part of the surface area of M1 (80%). The stepped morphology of the latter surface may generate similar metal-oxo arrangements as on the surface of the basal plane of the needles. HR-TEM studies together with targeted synthesis of M1 showing different microstructure are currently in progress to verify this assumption.

Acknowledgments

The authors thank Dr. Olaf Timpe for helpful discussions, Dr. Frank Girgsdies for performing the phase analysis of the catalysts, Edith Kitzelmann for conducting the XRD measurements, and Kilian Klaeden and Gisela Lorenz for carrying out the nitrogen adsorption measurements.

References

[1] T. Ushikubo, H. Nakamura, Y. Koyasu, S. Wajiki, US Patent 5 380 933 (1995), to Mitsubishi Kasei Corporation.
[2] M. Hatano, A. Kayo, US Patent 5 049 692 (1991), to Mitsubishi Kasei Corporation.
[3] T. Ushikubo, K. Oshima, A. Kayou, M. Hatano, Stud. Surf. Sci. Catal. 112 (1997) 473.
[4] M. Baca, A. Pigamo, J.L. Dubois, J.M.M. Millet, Top. Catal. 23 (2003) 39.
[5] J.M. Oliver, J.M. Lopez Nieto, P. Botella, Catal. Today 96 (2004) 241.
[6] W. Ueda, D. Vitry, T. Katou, Catal. Today 96 (2004) 235.
[7] H. Tsuji, K. Oshima, Y. Koyasu, Chem. Mater. 15 (2003) 2112.
[8] P. DeSanto Jr., D.J. Buttrey, R.K. Grasselli, C.G. Lugmair, A.F. Volpe Jr., B.H. Toby, T. Vogt, Z. Kristallogr. 219 (2004) 152.
[9] H. Murayama, D. Vitry, W. Ueda, G. Fuchs, M. Anne, J.L. Dubois, Appl. Catal. A Gen. 318 (2007) 137.
[10] A. Celaya Sanfiz, T.W. Hansen, F. Girgsdies, O. Timpe, E. Rödel, T. Ressler, A. Trunschke, R. Schlögl, Top. Catal. (2008), doi: 10.1007/s11244-008-9106-z, in press.
[11] W. Ueda, K. Oshihara, Appl. Catal. A 200 (2000) 135.
[12] K. Oshihara, T. Hisano, W. Ueda, Top. Catal. 15 (2001) 153.
[13] V.V. Guliants, R. Bhandari, R.S. Soman, O. Guerrero-Perez, M.A. Banares, Appl. Catal. A 274 (2004) 213.
[14] R.K. Grasselli, D.J. Buttrey, P. DeSanto Jr., J.D. Burrington, C.G. Lugmair, A.F. Volpe Jr., T. Weingand, Catal. Today 91–92 (2004) 251.
[15] V.V. Guliants, R. Bhandari, B. Swaminathan, V.K. Vasudevan, H.H. Brongersma, A. Knoester, A.M. Gaffney, S. Han, J. Phys. Chem. B 109 (2005) 24046.
[16] V.V. Guliants, R. Bhandari, A.R. Hughett, S. Bhatt, B.D. Schuler, H.H. Brongersma, A. Knoester, A.M. Gaffney, S. Hann, J. Phys. Chem. B 110 (2006) 6129.
[17] J.-P. Jacobs, A. Maltha, J.G.H. Reintjes, J. Drimal, V. Ponec, H.H. Brongersma, J. Catal. 147 (1994) 294.
[18] H.H. Brongersma, M. Draxler, M. de Ridder, P. Bauer, Surf. Sci. Rep. 62 (2007) 63.
[19] G. Mestl, N.F.D. Verbruggen, H. Knözinger, Langmuir 11 (1995) 3034.
[20] G.J.A. Hellings, H. Ottevanger, S.W. Boelens, C.L.C.M. Knibbeler, H.H. Brongersma, Surf. Sci. 162 (1985) 913.
[21] W.P.A. Jansen, A. Knoester, A.J.H. Maas, P. Schmitt, A. Kytökivi, A.W. Denier van der Gon, H.H. Brongersma, Surf. Interface Anal. 36 (2004) 1469.
[22] L.C.A. van den Oetelaar, H.E. van Benthem, J.H.J.M. Helwegen, P.J.A. Stapel, H.H. Brongersma, Surf. Interface Anal. 26 (1998) 537.
[23] M. Baca, A. Pigamo, J.L. Dubois, J.M.M. Millet, Top. Catal. 23 (2003) 39.
[24] R.K. Grasselli, D.J. Buttrey, J.D. Burrington, A. Andersson, J. Holmberg, W. Ueda, J. Kubo, C.G. Lugmair, A.F. Volpe Jr., Top. Catal. 38 (2006) 7.
[25] R.K. Grasselli, Catal. Today 99 (2005) 23.
[26] R.K. Grasselli, J.D. Burrington, D.J. Buttrey, P. De Santo, C.G. Lugmair, A.F. Volpe Jr., T. Weingand, Top. Catal. 23 (2003) 5.
[27] J.B. Wagner, O. Timpe, F.A. Hamid, A. Trunschke, U. Wild, D.S. Su, R.K. Widi, S.B.A. Hamid, R. Schlögl, Top. Catal. 38 (2006) 51.
[28] D. Vitry, Y. Moriwaka, J.L. Dubois, W. Ueda, Appl. Catal. A Gen. 251 (2003) 411.
[29] V.V. Guliants, R. Bhandari, H.H. Brongersma, A. Knoester, A.M. Gaffney, S. Han, J. Phys. Chem. B 109 (2005) 10234.
[30] H. Hibst, F. Rosowski, G. Cox, Catal. Today 117 (2006) 234.